ROSE 2010 - IEEE International Workshop on Robotic and Sensors Environments
Phoenix - Arizona, 15-16 October 2010

A Generic Configuration of a Compact Dexterous and Self-Contained End-Effector for Mobile Robotic Platforms

Paul M. Moubarak, Pinhas Ben-Tzvi, and Zhou Ma
Robotics and Mechatronics Laboratory
Department of Mechanical and Aerospace Engineering
The George Washington University
Washington DC, United States
Email: {paul4, bentzvi, mazhou}@gwu.edu

***Abstract*— This paper presents a new design of a compact end-effector for mobile robotic platforms that provides dexterous heavy duty gripping and handling of tasks by means of on-board manipulator arms. The merit of the proposed work lies in the novel concept we adopted in combining dexterity with strength and speed in a compact, self-contained and generic structure. The generic aspect of the design approach facilitates the implementation of this robotic end-effector on various manipulators with minor modifications to the overall robot structure. We discuss design layouts, capabilities and implementation aspects on manipulator arms of mobile robotic platforms.**

***Keywords:* Robotic hand, compact end-effector, self-contained, dexterity, field robotics**

I. INTRODUCTION

Mobile robots' ability to interact with their surroundings using manipulator arms and end-effectors is of integral importance for an effective accomplishment of an assigned task [1,2]. Traditionally, robotic end-effectors incorporated on mobile robotic platforms often imposed restrictions on the number of fingers and degrees of freedom due to design constraints, such as space and weight [3,4]. This in turn sacrificed critical aspects of the gripping capabilities and dexterity of the end-effector mechanism as a whole [5–7]. More recently, advances in pneumatic actuation culminated in the development of robotic end-effectors that employ a single central actuator to implement multiple degrees of freedom at the gripper level [8,9]. Dexterity levels comparable to the human hand can be achieved [10,11], where each finger is comprised of three phalanges actuated pneumatically [12]. However, despite the high level of dexterity that pneumatically actuated robotic hands can achieve, their implementation on mobile robotic platforms faces practicality challenges, often associated with the size of the air pump and compressor, or even the noise generated by the compressor fan and expanding air [13,14].

Cable-actuated robotic arms and end-effectors on the other hand, such as the WAM [15], are quieter, yet they can provide similar dexterity levels, which ultimately makes them more practical for indoor applications, such as house-keeping [16–18]. In all cases however, whether pneumatically, hydraulically [19] or cable actuated, the end-effector structure is not self-contained, in the sense that many external hardware components, such as pulleys, tensioners or solenoid valves need also to be integrated on the robot separately from the end-effector core structure. This requirement for extra space, however, does not improve payload capabilities. The payload-to-weight ratio is still low, in the sense that the end-effector can handle and maneuver objects that are at most five times heavier than its static weight. This aspect poses a practicality problem for field mobile robots that are often required to maneuver objects far heavier than the weight of the end-effector they carry on-board their manipulator arms. Ideally, a robotic hand should be capable of combining dexterity with strength, while maintaining a compact structure such that its functionality is not restricted to special-purpose indoor applications. Rather, it should be broadened to encompass field operations including search and rescue, reconnaissance, or even deep sea and deep space exploratory missions.

To tackle aspects of these challenges, we present a novel design for a self-contained robotic hand, with a compact structure and a gripping platform that accommodates several fingers and degrees of freedom. The hardware layout is generic, in the sense that it is designed to fit many manipulator arms with minor modifications to the core structure. The end-effector we present provides high payload capabilities, yet maintains structural compactness, which facilitates implementation on manipulator arms of mobile robots.

The paper is organized as follows: In Section II, we discuss the Mechanical layout and design specifications for the different mechanisms of the end-effector. In Section III, we emphasize the design of the electrical layout and discuss sensor and power requirements. In Section IV, we present the structural strength of the end-effector based on an FEA model of the assembly, and in Section V, we introduce a kinematic model of the hand. We then discuss implementation aspects on mobile robots and finally recapitulate our effort in a conclusion in Section VI.

II. MECHANICAL DESIGN

The end-effector illustrated in Figures 1, 2 and 3 is designed to carry a peak static load of 50Kg located at the fingertips of the gripping unit, and possesses the following overall dimensions: 89(H)×124(W)×257(L) mm. The mechanism comprises a fingers' module that accommodates up to four fingers. Each finger is driven by a worm gear

actuated by a single central worm that connects directly to a planetary gearhead. The latter provides a torque amplification ratio of 1:33 and is adapted directly to a Maxon flat brushless DC motor operating at a minimum of 12 Volts and providing a power of 30 Watts for a rated speed of 4370 RPM.

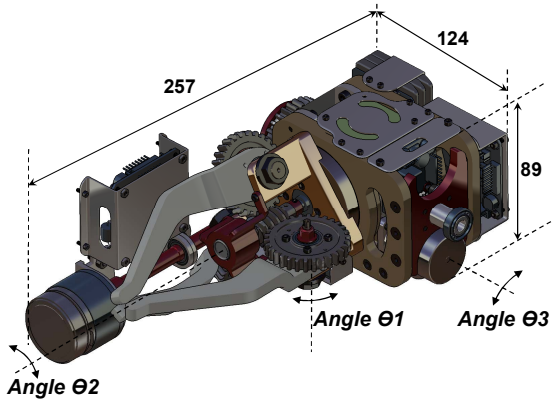

Figure 1. End-effector mechanism in the folded configuration with fingers closed.

The fingers' worm gear assembly provides an additional torque amplification ratio of 1:15, bringing the total ratio up to 1:495 at an overall transmission efficiency of 57%. The motor-gearhead assembly that drives the fingers (or angle Θ_1) is housed inside the wrist hollow hub and provides an angular rotation span of 0-110° for each finger at a peak angular velocity of 50°/sec. The fingers' motor can ultimately generate a peak gripping force of 120N at the fingertips.

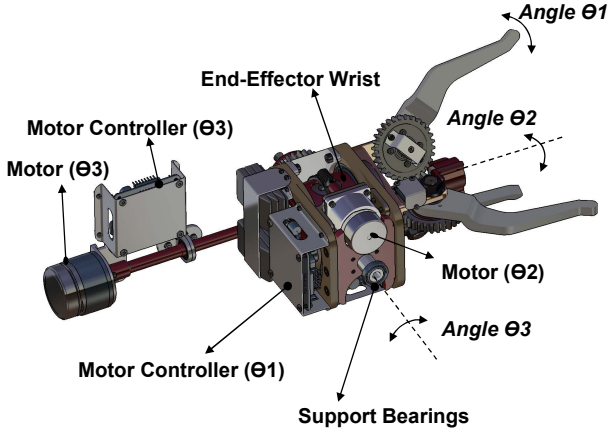

Figure 2. End-effector in the unfolded configuration with fingers opened.

An additional motor assembly connected to the wrist hub through another worm and worm gear assembly provides endless rotation of the fingers' module –as a whole– around the wrist centroidal axis. The motor that drives this degree of freedom (or angle Θ_2) is adapted to a spur gearhead, which provides a torque amplification ratio of 1:30. The worm gear assembly provides an additional 1:30 amplification factor for a total ratio of 1:900 and an overall transmission efficiency of 56%. In this case, a Maxon motor (Motor Θ_2) sitting on top of the wrist hub as shown in Figure 2 is also operated at a minimum of 12 Volts to provide 15 Watts of power at a rated speed of 4460 RPM. The dynamic torque available at this degree of freedom (angle Θ_2) if the motor is operated at 12 Volts is 12 Nm at an angular velocity of 30°/sec. However, peak torque values of 15 Nm at an angular velocity of 50°/sec are achievable when the motor is operated at higher voltages.

The third degree of freedom (angle Θ_3) is actuated by a motor and a spur gearhead assembly that rotates the whole mechanism around the support shafts. These shafts rest on two ball bearings that are housed inside the frame structure of a manipulator arm. Here again, we used a worm gear assembly with a 1:15 amplification ratio, which when combined with the 1:47 ratio provided by the spur gearhead, provides a total torque amplification factor of 1:705 and an overall transmission efficiency of 58%. The motor in this case is a replica of the one used to open and close the fingers, and hence possesses similar torque, speed and power characteristics. However, the peak torque requirements are different in this case, with a maximum of 21 Nm available for a peak angular velocity of 50°/sec. Here again, the motor can provide more power when operated at a higher voltage.

In all cases, the worm gear assembly provides in addition to torque amplification, means of self-braking for the articulated joints. Double-threaded worm gears provide robust mechanical locking to all degrees of freedom when idle, enabling the end-effector to lift and handle heavier objects, while concurrently saving the space required for additional electrical braking hardware. As such, the total calculated weight of the hand including all details shown in Figure 1 is 2.08 Kg when three fingers are adapted to the gripping platform.

For convenience, we conclude this paragraph with a summary of the mechanical and electrical specifications of the end-effector in Table 1.

TABLE I. SUMMARY OF THE MECHANICAL AND ELECTRICAL SPECIFICATIONS OF THE END-EFFECTOR FOR ALL THREE DOF'S

Specification	Angle Θ_1	Angle Θ_2	Angle Θ_3
Motor Power	30 W	15 W	30 W
Motor Rated RPM	4370	4460	4370
Motor Operating Voltage Range	12–18 V	12–18 V	12–18 V
Torque Amplification stages	2	2	2
Gearhead Ratio	1:33	1:30	1:47
Worm Assembly Ratio	1:15	1:30	1:15
Overall amplification factor	1:495(k_1)	1:900(k_2)	1:705(k_3)
Rated Final Output Torque	15.8 N.m	12 N.m	21 N.m
Transmission efficiency	57%	56%	58%
Rated Output Speed Range (under load)	50 –75°/s	30– 45°/s	50– 75°/s
Operating Angular Range	0 –110°	Endless	Endless
Motor Controller	EZSV23	EZSV17	EZSV23
Maximum Controller Current	5 A	2 A	5 A

III. ELECTRICAL DESIGN LAYOUT

In order to control the hand's motors, two controllers were incorporated within the structure. One controller (EZSV23, *AllMotion Inc.*) operates at 12–40Volts and is capable of providing up to 5Amp of continuous current. This controller (Motor Controller Θ_1) shown in Figure 2 commands the motor that opens and closes the fingers and is therefore located close to the motor electrical interface. On the other hand, an additional controller (Motor Controller Θ_2) shown in Figure 3 is embedded inside the end-effector structure, which commands the motor in charge of rotating the fingers platform around the centroidal axis of the wrist (angle Θ_2). This controller (EZSV17, *AllMotion Inc.*) operates at 20–40Volts and provides a continuous current of 2Amps.

Absolute encoders were implemented on all degrees of freedom in order to map and monitor the spatial position and orientation of the gripper mechanism. This includes a compact rotary analog encoder adapted directly to the fingers (Absolute Encoder Θ_1, *Bourns Inc.*), that provides an angular reading range of 0–330°. The reading from the encoder is transmitted to the end-effector's brain (Figure 3) via wireless RF communication, which eliminates any electrical wiring between the fingers' platforms and the brain, hence enabling endless rotation to the end-effector's wrist. To achieve this, an integrated X-Bee RF Module (*DIGI Inc.*, 2.4 GHz) with four A/D channels was implemented on the fingers platform. Another X-Bee (Figure 3) was similarly incorporated on the end-effector's brain to receive the encoder's signals. The brain of the hand includes a special-purpose circuit board housed on top of the frame. This board accommodates a 32-bit microcontroller (ARM7TDMI-S, *Philips*) and all necessary electronic hardware, such as switches and DC-DC voltage regulators.

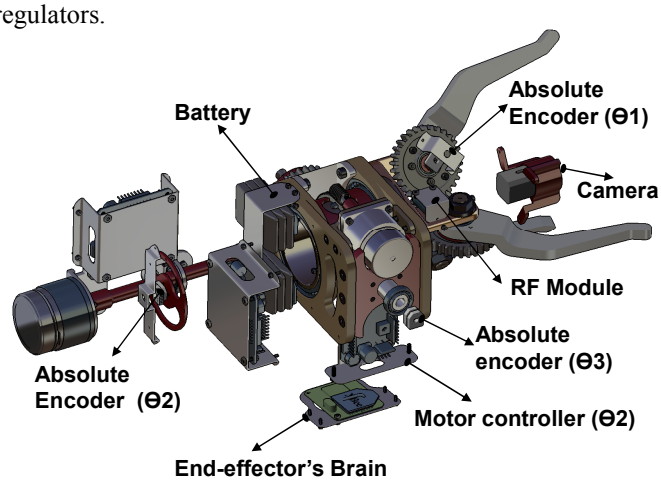

Figure 3. End-effector in the extended configuration showing electrical hardware details.

Absolute encoders such as the one described earlier were used to keep track of the second and third degree of freedom (Absolute Encoder Θ_2, Θ_3). However, since these degrees of freedom (Θ_2 and Θ_3) provide endless rotation, we cascaded two of the encoders on the same shaft to cover the full angular range of 0–360°. In this case too, the encoder pairs were adapted directly to the rotating shaft in order to provide a 1:1 ratio on the angular reading. It is worthwhile to mention that the fingers' platform also accommodates an analog high-quality color (*RF-Links Inc.*, 916MHz) wireless camera (Figure 3) for live video feed transmitted back to the remote operator. This visual data will enable the operator to perform remote handling maneuvers when manual operation is desired.

The end-effector also carries one 5-cell (AA Corp. PLH-703562, *Battery Space Inc.*) Li-Ion battery pack with 5Amps PCM (Protection Circuit Module) boards (Figure 3). Each cell nominally provides 3.7 Volts, and the serial configuration of these cells delivers a total of 18.5Volts at 1500 mAh. The battery provides power to local motors and all electrical hardware at a continuous current discharge of 3 Amps and a max current discharge of 5 Amps. This electrical performance is valuable considering the very compact size of one battery pack (65x39x32 mm) with an overall weight of 165 grams.

To control the end-effector's degrees of freedom, command signals generated by the robot main controller, or robot brain, are communicated wirelessly [20 – 22] to the end-effector's brain as shown in Figure 4, which then relays these signals to the motor controllers via wire means to perform the actuation. It is equally possible for an operator to control the robotic hand via a control unit (OCU). Commands generated by the OCU can be communicated to the robot brain through a 1Watt 9XTend module (at 900 MHz) and an X-Bee, which then relays the commands to the end-effector's brain through wireless interfacing (at 2.4 GHz).

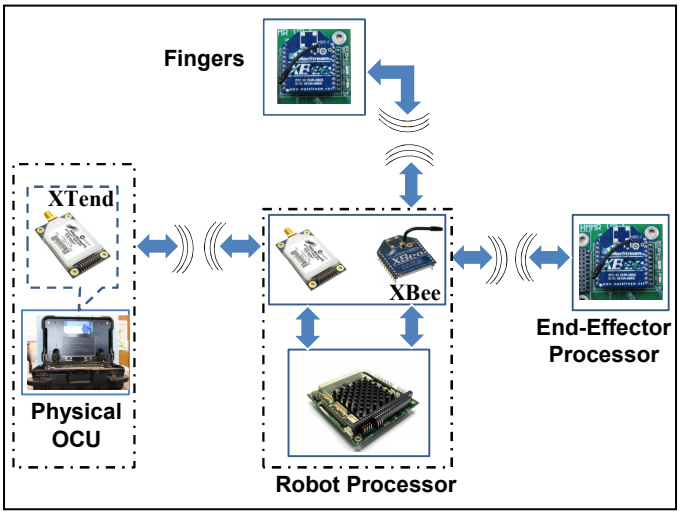

Figure 4. Communication protocol between the fingers, the gripper processing unit, the robot processing unit and the actual OCU.

With this mechanism established, additional sensors such as force feedback and shear sensors at the fingertips, as well as additional RF-module on the fingers platform can be easily mounted and interfaced to the on-board micro-controller and the robot brain via wireless communication. This ultimately provides a self-contained gripping platform we need for our current and future work on autonomous robotic handling and gripping functionalities.

IV. FINITE ELEMENT ANALYSYS

A finite element model of the end-effector was developed to briefly study the stress propagation through the structure under fingers loading. This enabled us to achieve ultimate design compactness and to minimize the total weight of the assembly while optimizing the payload capability. Because of the uncertainty in predicting the stress propagation from one part of the assembly to the other, an FEA analysis on the end-effector's assembly was favored over the analysis of individual parts. This approach yielded the most accurate results given the non-uniform and complex structure of the hand.

Figure 5 shows the propagation of stress from the fingers towards the support shafts for an applied load of 50Kg on a finger's tip. In this analysis, a clamp boundary condition was applied to the support shafts. All remaining parts in the assembly were constrained with respect to this clamp by defining appropriate surface constraints. To simplify the computational burden, we omitted from the analysis parts that do not contribute directly to the structural strength of the hand, such as motors and motor controllers, and parts that we can model on the solver platform such as the tightening force of a screw or a nut.

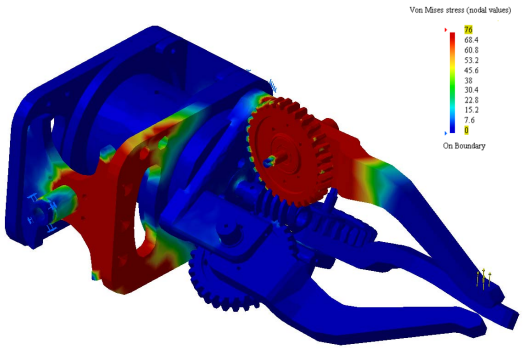

Figure 5. FEA contour plot on the geometry showing stress concentration and stress propagation through the hand for an applied finger load of 50Kg.

Using the Von Mises criterion [23], we depicted a peak stress of 76MPa concentrated on the loaded finger's worm gear. As can be seen in Figure 5, the end-effector's wrist did not experience significant loading. This is due to the worm and worm gear assembly in the center of the hand, which shielded the wrist, thereby preventing the transmission of axial load to the shaft of the motor located inside the wrist hub (motor angle Θ_1). As such, the load remained in majority bending and was propagated away from the fingers towards the support shafts. It should be noted that although the structural integrity of the end-effector proved strong enough to withstand a load of 50 Kg, in reality, the hand's mechanical power cannot maneuver such heavy load. Maneuvering in this case will be performed by the on-board manipulator arm, which this hand will be mounted on. In this case, the hand will only provide static locking to all joints preventing any unwanted motion of the load.

Material selection and final dimensioning was ultimately completed based on these FEA results, where steel was chosen for critically stressed parts and aluminum for less stressed parts, resulting in a total assembly weight of 2.08 Kg.

V. KINEMATIC MODEL OF THE END-EFFECTOR

The kinematic model of the end-effector includes three rotational degrees of freedom revolving around three different axes as illustrated in Figures 6 and 7. These degrees of freedom or joints are driven by motor-gearhead assemblies using worm gears. To present the kinematic model of these joints, we first formulate the following definitions.

We define:

- ω_1 as the rotational speed of the motor that drives angle Θ_1
- ω_2 as the rotational speed of the motor that drives angle Θ_2
- ω_3 as the rotational speed of the motor that drives angle Θ_3

We also define k_1, k_2 *and* k_3 as the overall amplification ratios achieved by the gearhead and the worm gear assembly of every motor-unit driving angles Θ_1, Θ_2 and Θ_3 respectively. Therefore, the angular velocities of the joints, denoted $\dot{\Theta}_1$, $\dot{\Theta}_2$ and $\dot{\Theta}_3$ can be written as a function of the motors' rotational speed as follows:

$$\dot{\Theta}_1 = \frac{\omega_1}{k_1} \quad with\ k_1 = 495 \tag{1}$$

$$\dot{\Theta}_2 = \frac{\omega_2}{k_2} \quad with\ k_2 = 900 \tag{2}$$

$$\dot{\Theta}_3 = \frac{\omega_3}{k_3} \quad with\ k_3 = 705 \tag{3}$$

where k_1, k_2 and k_3 were defined in Table 1.

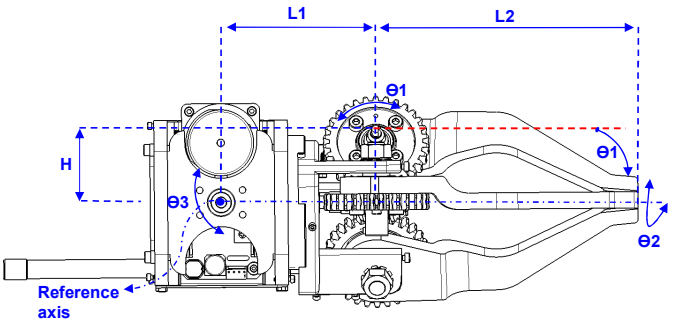

Figure 6. Schematic illustration showing the side view of the gripper with the rotational degrees of freedom.

Achieving autonomous handling maneuvers using the hand requires a fundamental knowledge of the spatial location of points of interest on the hand with respect to a global stationary frame. For our application, we chose the fingertips as points of interest since they represent the maximum spatial reach the end-effector mechanism can achieve. Other points of

the hand, such as the center of mass, can be calculated with respect to the fingertips once the kinematics of the latter are developed. As to the reference coordinate system, we chose the planes orthogonal to the axis of rotation of joint Θ_3 since this axis is the one around which the whole hand revolves, and therefore is stationary with respect to the assembly.

We then define the distance between the vertical plane and the axis of rotation of angle $\Theta_1$as L_1. Likewise, we define the length of a finger from the joint to the tip by L_2 and the vertical component separating the axis of rotation of joint Θ_1 from the central axis by H, as shown in Figure 6. The X, Y and Z coordinate axes are illustrated in Figure 7. We note that the Z-axis is orthogonal to the profile plane of the hand and thereby follows the right hand rule where the positive Z-direction is pointing outward from the plane of the figure.

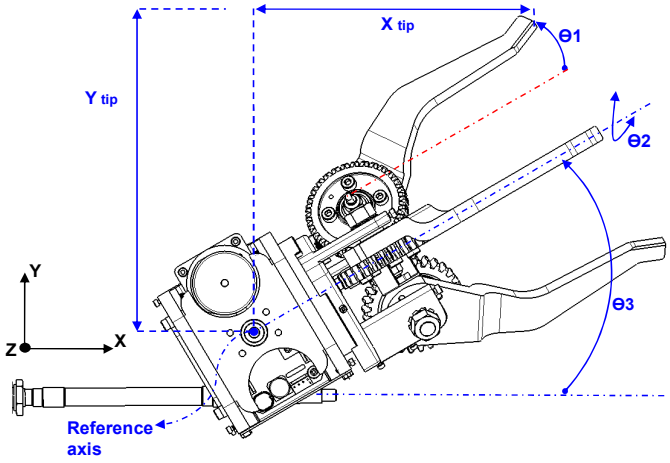

Figure 7. Side view of the hand showing kinematic details.

Angle Θ_1 is measured with respect to a horizontal line running through the joint's axis of rotation. Clockwise rotation is considered negative, while counterclockwise rotation is positive. As such, angle $\Theta_1 = 0°$ when the tip of the respective finger is aligned with this reference axis (red dashed line in Figures 6 and 7). Angle Θ_2 is measured with respect to the vertical axis (Y-axis) while angle Θ_3 is measured with respect to the horizontal axis (X-axis) following the right hand rule for sign convention.

We denote the coordinates of a fingertip with respect to the reference frame as X_{tip}, Y_{tip} and Z_{tip} as shown in Figure 7. These coordinates can be expressed as a function of the joint angles Θ_1, Θ_2 and Θ_3 using Denavit–Hartenberg parameters or trigonometric identities. This can be more conveniently achieved based on a simplified schematic illustration of the hand links and joints as shown in Figure 8. The kinematic model of the gripper can therefore be expressed as:

$$\boldsymbol{X_{tip}} = L_1 \cos(\Theta_3) + L_2 \cos(\Theta_1) \cos(\Theta_3) - \{H + L_2 \sin(\Theta_1)\} \cos(\Theta_2) \sin(\Theta_3) \quad (4)$$

$$\boldsymbol{Y_{tip}} = L_1 \sin(\Theta_3) + L_2 \cos(\Theta_1) \sin(\Theta_3) + \{H + L_2 \sin(\Theta_1)\} \cos(\Theta_2) \cos(\Theta_3) \quad (5)$$

$$\boldsymbol{Z_{tip}} = L_2 \sin(\Theta_1) \sin(\Theta_2) + H \sin(\Theta_2) \quad (6)$$

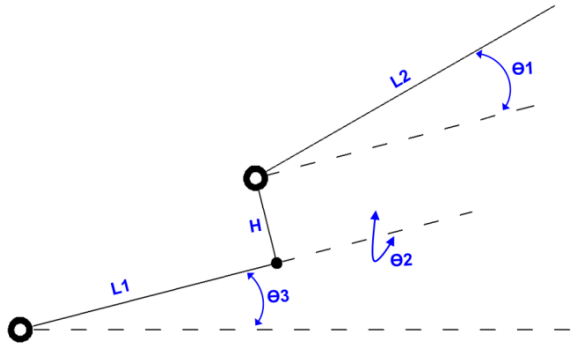

Figure 8. Simplified schematic representation of the hand's links and joints.

The above equations have to satisfy the following kinematic constraints:

- $-15° \leq \Theta_1 \leq 95°$ (a)
- $0° \leq \Theta_2 \leq 360°$ (b)
- $0° \leq \Theta_3 \leq 360°$ (c)
- $0° \leq \Theta_1 \leq 10°$ if $90° \leq \Theta_3 \leq 270°$ (d)

Constraint (d) is required to ensure that the fingers are in a compact configuration when the gripper is rotated to fold inside a manipulator arm (a configuration similar to one shown in Figure 1). This is required to avoid any clashing with surrounding components in the robot and ensure smooth continuous rotation of the hand around joint Θ_3.

The kinematic equations are clearly non-linear. Therefore, given a desired position of the fingertips $(X_{tip}, Y_{tip}, Z_{tip})$ as dictated by the location of the object to be handled, eq. (4), (5) and (6) can be solved and satisfied for a large number of possible combinations of angles Θ_1, Θ_2 and Θ_3. Discussing the algorithm that computes an optimal configuration in real time based on visual sensor input does not fall within the scope of this paper, but constitutes a major component of our prospective research on autonomous manipulation with the established mechanism.

VI. Conclusion and Future Implementations

This paper presented the design of a compact hand (89(H)×124(W)×257(L) mm) for heavy-duty robotic handling and gripping applications. The hand we presented is self-contained in the sense that it encompasses all mechanical, structural, electrical hardware in one compact structure, hence making it easy to implement on a variety of manipulator arms with minor modifications to the core structure. The structural strength of the end-effector's assembly based on an FEA model was discussed, and a kinematic model of the three rotational degrees of freedom which yielded non-linear equations with no trivial solutions was presented.

With these results established, future work will focus on the implementation aspect on robotic manipulators of mobile

robots [24 – 26]. A sample implementation is shown in Figure 9, where the hand is incorporated on the end-link of a manipulator arm.

Future work will also investigate the development of algorithms that calculate the optimal configuration of the joint angles for a given position and shape of the object to be handled. This includes identification of the target object via object sensing and image processing, accurate positioning and adequate handling with tactile feedback in order to achieve autonomy for gripping maneuvers carried by mobile robots.

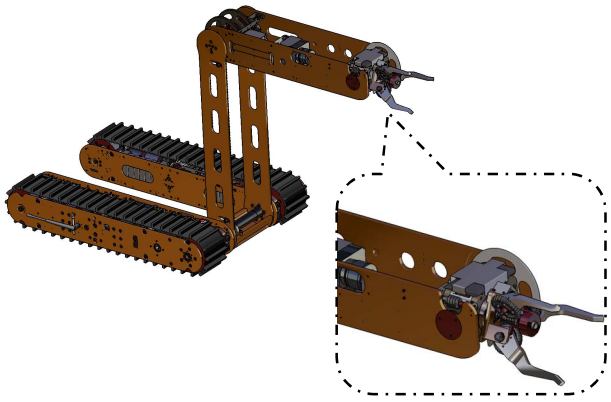

Figure 9. Implementation of the hand on the manipulator arm of a sample mobile robot.

ACKNOWLEDGMENT

This work is supported by the Defense Advanced Research Program Agency (DARPA) under grant number R0011-09-1-0049. We also would like to acknowledge the support provided by the DARPA Program Manager, Ms. Melanie Dumas.

REFERENCES

[1] Z. Xu, T. Deyle and C.C. Kemp, "1000 Trials: An empirically validated end effector that robustly grasps objects from the floor", IEEE Int. Conference on Robotics and Automation, Japan, pp. 3971 – 3978, 2009,

[2] J. Ueda, M. Kondo and T. Ogasawara, "The multifingered NAIST hand system for robot in-hand manipulation", J. Mechanism and Machine Theory, Vol.45, No. 2, pp. 224 – 238, 2010.

[3] L. Birglen and C.M. Gosselin, "Grasp-state plane analysis of two-phalanx underactuated fingers", J. Mechanism and Machine Theory, Vol.41, No. 7, pp. 807 – 822, 2006.

[4] M. Ceccarelli, I. Luyckx and W. Vanaelten, "Grasp forces in two-finger grippers: modelling and measuring", 5th International Workshop on Robotics, Budapest, pp. 321 – 326, 1996.

[5] G. Carbone, S. Iannone and M. Ceccarelli, "Regulation and control of LARM hand III", J. Robotics and Computer-Integrated Manufacturing, Vol.26, No. 2, pp. 202 – 211, 2010,

[6] J. Butterfass, M. Fischer, M. Grebenstein, S. Haidacher and G. Hirzinger, "Design and experiences with DLR hand II, robotics: trends, principles, and applications", Proceedings of the 6th Biannual World Automation Congress (WAC 2004), Spain, pp. 105–110, 2004.

[7] A. Rovetta, "Design and control of mechanical hands for robots", Computers in Industry, Vol.7, No.3, pp. 275 – 282, 1986,

[8] T. Lalibert´e and C.M. Gosselin, "Simulation and design of underactuated mechanical hands", J. Mechanism and Machine Theory, Vol.33, No. 1-2, pp. 39 – 57. 1998,

[9] S. Nishino, N. Tsujiuchi, T. Koizumi, H. Komatsubara, T. Kudawara and M. Shimizu, "Development of Robot Hand with Pneumatic Actuator and Construct of Master-Slave System", Proceedings of the 29th Annual International Conference of the IEEE Engineering in Medicine and Biology Society, pp. 3027 – 3030, 2007.

[10] M. Reichel, "transformation of Shadow dextrous hand and Shadow finger test unit from prototype to product for intelligent manipulation and grasping", The Shadow Robot Company, Proceedings of the International Conference on Intelligent Manipulation and Grasping, Italy, 2004,

[11] The shadow dexterous hand, http://www.shadowrobot.com/hand/, retrieved on June 2010.

[12] Y. Liu, A. Hoover and I. Walker, "Dynamic intercept and manipulation of objects using a novel pneumatic robot hand", Proceedings of the 12th International Conference on Advanced Robotics, Seattle WA, pp. 129 – 134, 2005,

[13] N. Tsujiuchi, T. Koizumi, S. Shirai, T. Kudawar and Y. Ichikawa, "Development of a low pressure driven pneumatic actuator and its application to a robot hand", Proceedings of the IEEE 32nd Annual Conference on Industrial Electronics, IECON '06 , France, pp. 3040 – 3045, 2006.

[14] A. Bierbaum, J. Schill, T. Asfour and R. Dillmann, "Force position control for a pneumatic anthropomorphic hand", Proceedings of the 9th IEEE-RAS International Conference on Humanoid Robots, France, pp. 21 – 27. 2009,

[15] The Barret Hand™ http://www.barrett.com/robot/products-hand.htm, retrieved June 2010.

[16] S.K. Mustafa, G. Yang, S. H. Yeo, W. Lin and I. Chen, "Self-calibration of a biologically-inspired cable-driven robotic arm", Proceedings of the IEEE/ASME International conference on Advanced Intelligent Mechatronics, Switzerland, pp. 1 – 6, 2007.

[17] L. Zollo, B. Siciliano, C. Laschi, G. Teti and P. Dario, "An experimental study on compliance control for a redundant personal robot arm", J. Robotics and Autonomous Systems, Vol.44, No. 2, pp. 101 – 129, 2003.

[18] S. Wang, L. Yue, Q. Li and J. Ding, Conceptual design and dimensional synthesis of 'MicroHand', J. Mechanism and Machine Theory, Vol.43 No.9, pp. 1186 – 1197, 2008.

[19] A. Garcia-Cerezo, A. Mandow, J.L. Martinez, J. Gomez-de-Gabriel, J. Morales, A. Cruz, A. Reina and J. Seron, "Development of ALACRANE: A mobile robotic assistance for exploration and rescue missions", Proceedings of the IEEE International Workshop on Safety, Security and Rescue Robotics, Italy, pp.1 – 6, 2007.

[20] P. Ben-Tzvi, A.A. Goldenberg, J.W. Zu, "Articulated Hybrid Mobile Robot Mechanism with Compounded Mobility and Manipulation and On-Board Wireless Sensor/Actuator Control Interfaces", J. Mechatronics, Vol.20, No.6, pp. 627 – 639, 2010.

[21] P. Ben-Tzvi, A.A. Goldenberg, J.W. Zu, "A Novel Control Architecture and Design of Hybrid Locomotion and Manipulation Tracked Mobile Robot", Proceedings of the 2007 IEEE International Conference on Mechatronics and Automation (ICMA 2007), China, pp. 1374 – 1381, 2007.

[22] P. Ben-Tzvi, A.A. Goldenberg, J.W. Zu, "Implementation of Sensors and Control Paradigm for a Hybrid Mobile Robot Manipulator for Search and Rescue Operations", Proceedings of the 2007 IEEE International Workshop on Robotic and Sensors Environments (ROSE 2007), Canada, pp. 9 – 97, 2007.

[23] R. Von Mises, *Mechanik der Festen Korper im plastisch deformablen Zustand*. Göttin. Nachr, Math. Phys., Vol. 1, pp. 582 – 592, 1913.

[24] P. Ben-Tzvi, "Experimental Validation and Field Performance Metrics of a Hybrid Mobile Robot Mechanism", J. Field Robotics, Vol.27, No. 3, pp. 250 – 267, 2010.

[25] P. Ben-Tzvi, A.A. Goldenberg, J.W. Zu, "Design and Analysis of a Hybrid Mobile Robot Mechanism with Compounded Locomotion and Manipulation Capability", Transactions of the ASME, J. Mechanical Design, Vol.130, pp. 1 – 13, 2008.

[26] P. Ben-Tzvi, A.A. Goldenberg, J.W. Zu, "Design, Simulations and Optimization of a Tracked Mobile Robot Manipulator with Hybrid Locomotion and Manipulation Capabilities", Proceedings of the 2008 IEEE International Conference on Robotics and Automation (ICRA2008), California, pp. 2307 – 2312, 2008.